Int. J. Heat Mass Transfer. Vol. 27, No. 10, pp. 1691 1700, 1984
Printed in Great Britain

0017-9310/84 $3.00 + 0.00

Parametric effects on the onset of flooding in flat-plate geometries

S. C. LEE and S. G. BANKOFF
Mechanical and Nuclear Engineering Department, Northwestern University, Evanston, IL 60201, U.S.A.

(*Received* 19 *May* 1983 *and in revised form* 30 *November* 1983)

Abstract—Flooding of countercurrent stratified steam water flow in flat-plate geometries is investigated. Both local and global effects of condensation on the onset of flooding are discussed, based on the results of top and bottom flooding tests. The influence of the channel depth and inclination angle on the flooding velocity is also explored. An envelope model, which considers flooding to be the limiting condition for countercurrent flow, is presented and compared with extensive data at various inclinations. Quite good agreement is shown at the nearly horizontal and moderately steep inclinations, but the onset of flooding in nearly vertical flow is expedited by significant droplet entrainment, and thus takes place earlier than the theory predicts.

INTRODUCTION

FLOODING in countercurrent gas–liquid flow is an important phenomenon in a variety of industrial applications such as tubular reflux condensers, film separators, and tubular contactors. In recent years, interest in the flooding phenomenon has grown in connection with the safety analysis of nuclear reactor systems. Flooding may limit the penetration of emergency coolant into a hot reactor core during a postulated loss-of-cooling accident (LOCA) in either a boiling-water reactor (BWR) equipped with a spray system, or a pressurized-water reactor (PWR) with an upper head injection system. Much effort has been devoted to improving the understanding of flooding in connection with the performance of nuclear reactor safety systems [1].

Previous studies of flooding may be classified into three different categories: onset of flooding, partial delivery, and hanging film (zero penetration) phenomena. Many studies have dealt with the prediction of the onset of flooding in vertical annular flow. The onset of flooding, sometimes called countercurrent flow limitation, refers to the limiting condition where the flow rates of neither the gas nor the liquid phase can be increased further without altering the flow pattern. Flooding in stratified flow may be of interest in conjunction with the injection of emergency core cooling water in the PWR hot leg between the steam generator and the reactor vessel in a small-break accident. Further, a study of this flow configuration may provide an important addition to our understanding of the flooding process, since independent variations of void fraction, aspect ratio and inclination angle are possible in this mode.

The characteristics of the flooding phenomenon are dependent upon various parameters, such as tube-end geometries, tube diameter (channel depth in rectangular or square ducts), properties of fluids used, and method of operation. Among these, the effect of tube-end geometry appears to be critical in determining the flooding velocity. It has been shown that the gas flooding velocity is substantially reduced if the liquid film is not introduced smoothly to the tube [1]. Furthermore, the end effects play a significant role in determining the locus of the onset of flooding, which is of great importance in steam/subcooled-water flow because of condensation. If a smooth liquid film is introduced, the onset of flooding takes place at the bottom of the tube (bottom flooding), while the introduction of a rough liquid film causes flooding to initiate at the top (top flooding).

The effect of the tube diameter or channel depth has been of central interest, associated with the development of possible scaling laws in single-channel flows. The best-known scaling parameters for vertical single-tube flooding are the Wallis and Kutateladze numbers [2, 3]. The Wallis number, defined by equation (1), represents the ratio of inertia force to hydrostatic force, whereas the length scale in the Wallis number is simply replaced by the Laplace constant to obtain the Kutateladze number

$$J_k^* = j_k\left[\frac{\rho_k}{(\rho_f-\rho_g)gD}\right]^{1/2}. \quad (1)$$

However, a completely satisfactory scaling law with these parameters has not yet been established, partly because not enough data with consistent test conditions are yet available, and partly because the diameter effect may be more complicated than these parameters indicate [1]. Scaling tests with stratified flow in rectangular ducts may be useful because of the simplicity and flexibility mentioned above. Data in this flow configuration, however, are very rare at the present time.

The present work deals with stratified steam–water flow in rectangular ducts inclined at various angles to the horizontal. Local and global effects of condensation on the onset of flooding are discussed, based on top and bottom flooding tests. The effects of the channel depth and inclination angle are investigated using two

NOMENCLATURE

D tube diameter [m]
f friction factor or condensation efficiency
H channel depth [m]
H^* dimensionless channel depth, $2H[(\rho_f-\rho_g)g \sin\theta/\sigma]^{1/2}$
h heat transfer coefficient [kW m^{-2} K^{-1}]
i_{fg} latent heat [kJ kg^{-1}]
j superficial velocity [m s^{-1}]
J^*_{mk} modified Wallis parameter defined in equation (7)
K dimensionless subcooling number, $C_{pl}(T_s-T_f)/i_{fg}$
L channel length [m]
N_{mk} modified two-phase Grashof number, $[2gH^3 \sin\theta\rho_k(\rho_f-\rho_g)/\mu_k^2]^{1/2}$
Nu Nusselt number, $h\delta/k_f$
Nu^* Nusselt number, hx/k_f
Pr Prandtl number, ν_f/α_f
Re Reynolds number, W/μ
St Stanton number, $Nu^*/(Pr\,Re_f)$
U average velocity [m s^{-1}]
W mass flow rate per unit width [kg m^{-1} s^{-1}]
x streamwise coordinate [m]
x^* dimensionless streamwise coordinate, x/L.

Greek symbols

α void fraction or thermal diffusivity [m^2 s^{-1}]
β ratio of interface velocity to average liquid velocity
δ mean film thickness [m]
δ^* dimensionless film thickness
θ inclination angle
θ^* inclination angle causing maximum flooding velocity
μ viscosity [N s m^{-2}]
ν kinematic viscosity [m^2 s^{-1}]
ρ density [kg m^{-3}]
σ surface tension [N m^{-1}].

Subscripts

a adiabatic
e effective
f liquid
g gas
i interface
in inlet
k g or f
L total length
out outlet
s saturation
w wall.

different aspect ratios and three inclinations. The similarities and differences of the flooding process at these inclinations are also discussed. In addition, a flooding analysis based on the envelope of possible operating lines, using the hydrodynamic and energy equations for inclined countercurrent stratified flow, is presented and compared with the data for the onset of flooding.

EXPERIMENTAL SYSTEM AND PROCEDURE

A schematic diagram of the experimental apparatus is shown in Fig. 1. It consists of a test section, steam supply line and circulating-water loop. The test section was basically designed to assure reasonably two-dimensional (2-D) stratified countercurrent flow and also to allow different aspect ratios by replacing the sidewalls. It is a rectangular channel approximately 2.13 m long and 0.38 m wide. The distance between the water inlet and outlet is 1.27 m. The test section has its own support system which permits any inclination between 0° and 90°. Two channel depths ($H = 0.076$ and 0.038 m) and three inclination angles ($\theta = 4.5°$, $\sim 30°$, 87° from the horizontal) were used.

The steam comes from the building supply, which is nominally saturated and at a pressure of 1.02 MPa. A steam separator and throttling valve assure dry, superheated steam at the entrance to a manifold of flow measurement venturis with a diameter of either 3.18 or 5.08 cm. The absolute pressure and temperature are monitored at the venturis to determine the thermodynamic condition of the incoming steam. When the steam enters the test section, a uniform flow is maintained by means of a perforated plate and honeycomb assembly in the lower plenum and is then discharged to the atmosphere at the top of the test section. Normally the steam has 10–40°C superheat at the entrance and was assumed to be at 1 atm pressure (0.1 MPa) for calculating its properties.

The water, by contrast, flows in a closed loop, which includes two storage tanks, a heat exchanger, two circulating pumps, and a 3.18 cm diameter venturi. The water is introduced through a stainless steel porous plate into the test section and discharged by gravity through a fine-mesh screen in the lower plenum. A guide vane is used at the water entrance to maintain a smooth and uniform film. This geometry minimized tube-end effects, resulting in flooding initiating at the

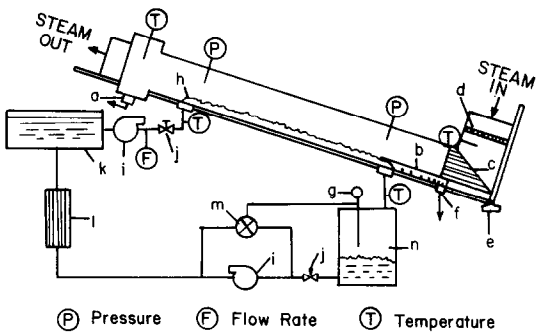

FIG. 1. Schematic diagram of experimental apparatus: (a) bypass liquid outlet; (b) divider wall; (c) honeycomb; (d) perforated plate; (e) journal bearing; (f) auxiliary drain; (g) level meter; (h) guide vane; (i) pump; (j) control valve; (k) storage tank; (l) heat exchanger; (m) solenoid valve; (n) water holding tank.

liquid exit (bottom flooding). However, the vane was removed when introduction of an artificial rough liquid film was needed for top-flooding tests. Hot water discharged from the test section is collected in a holding tank whose water level is controlled by a bypass solenoid control valve. The water inlet temperature can be regulated over the range of 7–98°C by varying the coolant rate in the heat exchanger.

The temperatures of the steam and the water are measured with chromel–alumel thermocouples at the inlet and outlet. The probes are of the ungrounded junction type, enclosed within a 1.6 mm stainless steel sheath, connected to a reference junction. The calibration of thermocouples showed agreement within ± 1°C. Pressure taps 0.25 mm in diameter allow pressure drop measurement in order to detect the onset of flooding. The steam flow rate is calculated using the equation of state and the isentropic energy equation, based upon the measurements of thermodynamic state and pressure drop at the venturi. It showed agreement with the calibrated flow rate within an accuracy of $\pm 2\%$. The signals from the thermocouples, transducers, and flowmeters are processed by a PDP 11-34 computer interfaced with a 16-channel AR-11 A/D converter. This computer-based data acquisition system has a maximum scan rate of approximately 30 kHz and a maximum scan repeat rate of 250 Hz. More details on the apparatus and instruments are found elsewhere [4].

The data for onset of flooding were obtained by increasing the steam flow rate at a given water flow rate. The onset of flooding was determined mainly by visual observation, but occasional checks by means of pressure drop measurements were made to assure the reliability of the data. When the flooding point was approached, sudden increases in pressure drop were observed, similar to those observed in adiabatic flow. Details on the pressure drop characteristics in countercurrent steam/subcooled-water are discussed in the preceding paper [5].

THEORETICAL CONSIDERATIONS

Efforts to explore the initiation and the basic mechanism of flooding have been made by a number of investigators, both theoretically and experimentally, over the years. Several different viewpoints on the onset of flooding in single-tube countercurrent gas–liquid flow have been suggested, which are described in detail by Bankoff and Lee [1]. Some consider flooding to be the result of interfacial instability between two superposed fluids flowing at different velocities. This viewpoint focuses attention on the circumstances under which the interfacial waves tend to grow with time. Various assumptions, such as potential flow [6] and viscous laminar flow [7], have been used in developing these models. However, a purely theoretical approach is very difficult, and most investigators have therefore set up simplified equations with extensive idealizations and/or used some empirical equations for the countercurrent flow parameters. The models are, in general, based on linear stability theory, which may be of limited usefulness in light of experimental evidence that the finite-amplitude surface waves dominate on a vertically falling liquid film [8, 9]. For pure gravity waves, Mishima and Ishii [10] showed that the critical gas velocity based on Kelvin–Helmholtz instability theory increases by a factor of approximately two, compared to that based on finite-amplitude stability analysis.

From another viewpoint, flooding is the limiting condition for countercurrent flow, which suggests an envelope theory based upon the steady hydrodynamic equations. Usually the envelope is taken to be the locus of tangents to the operating lines in the (j_g, j_f) plane for constant void fraction, and hence represents a limiting curve separating the operating region from an unattainable region for countercurrent flow. Physically, a large-amplitude wave appears on the interface during the development of flooding flow, resulting in a sharp increase of the effective roughness of the moving gas–liquid interface, and thus the interfacial shear stress. This acts to push the liquid film backwards, retarding the liquid downflow and leading to the onset of flooding. The limit of countercurrent flow corresponds to the retardation of the liquid film due to the interfacial shear stress. Therefore, the interfacial friction factor is a key parameter in this analysis. The theory has the advantage that it can be extended to the flooding analysis of condensing flows if the pertinent correlations for local heat transfer are known. Further, it may be used in various geometries, such as vertical annular flow [11], inclined stratified flow [5], and presumably countercurrent flow in porous media or in multiple channels, providing that appropriate empirical friction factor relationships are available.

The envelope theory is used to account for the onset of flooding in inclined countercurrent stratified steam–water flow in this study. Flooding equations based on this theory have been derived in a previous paper [5]. The flooding curve for countercurrent stratifed

condensing two-phase flow can be obtained by eliminating the void fraction from the following equations

$$F(J^*_{mg}, J^*_{mf}, \alpha) = \frac{f_{wg}J^{*2}_{mg}}{\alpha^3} + \frac{f_{wf}J^{*2}_{mf}}{(1-\alpha)^3} + \frac{f_{ia}}{\alpha(1-\alpha)} \times \left[\frac{J^*_{mg}}{\alpha} + \beta\left(\frac{\rho_g}{\rho_f}\right)^{1/2} \frac{J^*_{mf}}{(1-\alpha)}\right]^2 + 2\left(\frac{H}{L}\right)\left[\frac{(2\alpha-1)}{\alpha^2(1-\alpha)} J^*_{mg} + 2\left(\frac{\rho_g}{\rho_f}\right)^{1/2} \frac{J^*_{mf}}{(1-\alpha)^2} + 2\left(\frac{H}{L}\right)^2 \left(\frac{d^2J^*_{mg}}{dx^{*2}}\right)\right]\left(\frac{dJ^*_{mg}}{dx^*}\right) - 1 = 0 \quad (2)$$

$$G(J^*_{mg}, J^*_{mf}, \alpha) = \frac{\partial F}{\partial \alpha} = 0 \quad (3)$$

where

$$\frac{dJ^*_{mg}}{dx^*} = \frac{1}{x^*}\left(\frac{\rho_f}{\rho_g}\right)^{1/2} St\,[(1+K)J^*_{mf,in} - J^*_{mf}] \quad (4)$$

$$\frac{d^2J^*_{mg}}{dx^{*2}} = -\frac{1}{x^*}\left[1 + St + \frac{x^*}{St}\frac{dSt}{dx^*}\right]\frac{dJ^*_{mg}}{dx^*} \quad (5)$$

and the Stanton number is defined by

$$St = \frac{Nu^*}{Pr\, Re_f}. \quad (6)$$

Equation (2) is a combined form of dimensionless momentum equations for vapor and liquid phases, and equations (4) and (5) are basically dimensionless heat transfer equations. In this analysis, a modified Wallis parameter, for k-phase, J^*_{mk}, which considers the effect of inclination angle, was introduced

$$J^*_{mk} = j_k\left[\frac{\rho_k}{2gH\sin\theta(\rho_f - \rho_g)}\right]^{1/2} \quad (7)$$

where the hydraulic diameter of the test section is chosen as the length scale. In equations (2) and (4), the adiabatic interfacial friction factor and Stanton number should be furnished empirically. Empirical correlations used in this study are listed in the Appendix.

CONDENSATION EFFECT

The influence of condensation on the onset of flooding may be considered in terms of both local and global effects. The local effect is associated with the change of the vapor flooding velocity due to local condensation heat transfer. One is here concerned with the deviation of the local properties of the interfacial waves in condensing flow from those in adiabatic flow. However, this may be insignificant in most practical cases, and an explicit theoretical approach appears to be difficult. On the other hand, considerations of the global effect focus on the calculation of the effective steam flow rate to initiate flooding. This effect is of practical interest, particularly in conjunction with steam–water countercurrent flow in nuclear reactor safety systems [12–14]. The effective steam flow rate is not, in general, equal to the steam supply rate, unless the locus of flooding is the bottom of the tube. If flooding is initiated at some other location, the reduction of the steam flow rate due to condensation must be considered.

Bottom flooding data at several initial liquid subcoolings in nearly horizontal countercurrent steam–water flow are shown in Fig. 2. The prediction by

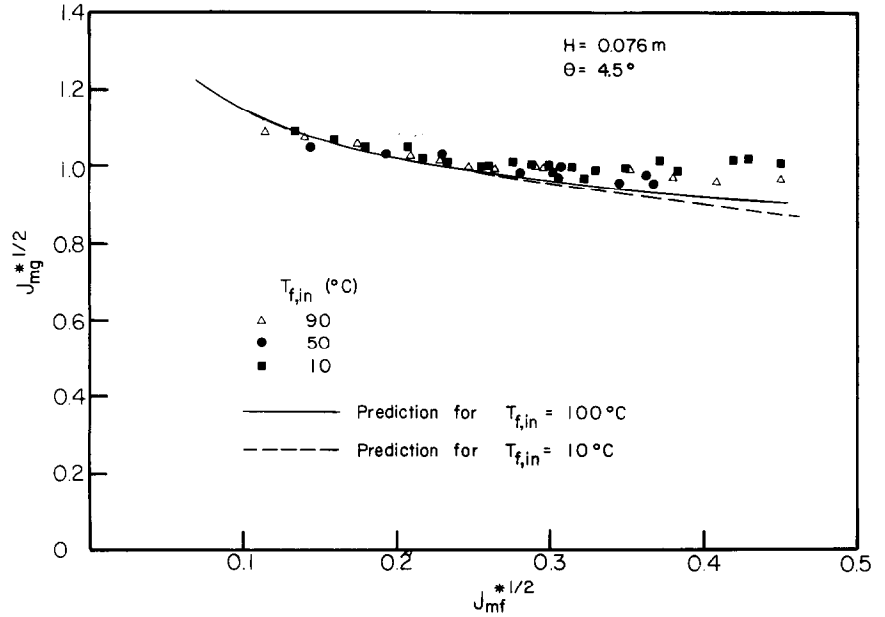

FIG. 2. Comparison of envelope theory with bottom flooding data in nearly horizontal flow.

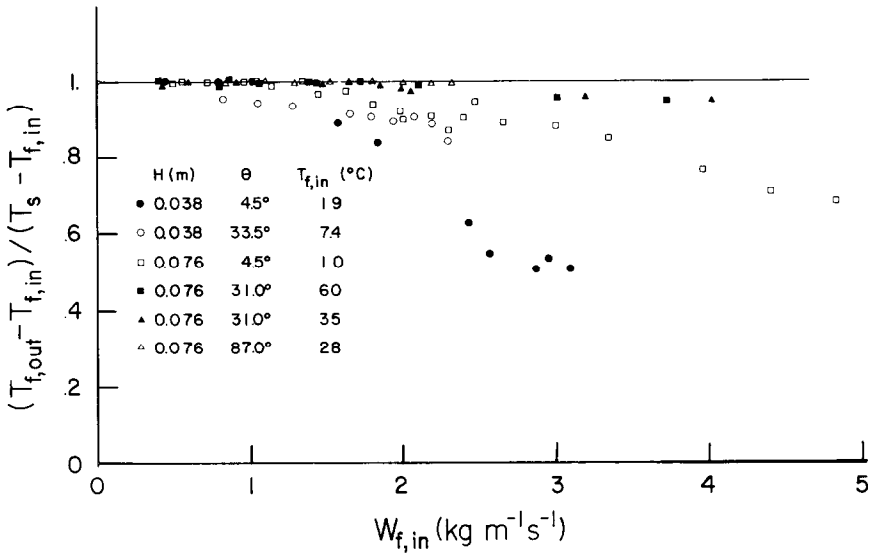

FIG. 3. Dimensionless water outlet temperatures for bottom flooding data.

the envelope theory is also indicated in this illustration. It is seen that the vapor flooding velocity for bottom flooding appears to be relatively insensitive to the water entrance temperature. The same result is indicated for other geometrical conditions, as seen in Figs. 6 and 8. This is evidently because the exit water is nearly saturated, regardless of the water inlet temperature, so that the flooding characteristics are similar to those of air–water flow. Figure 3 shows the dimensionless water outlet temperature for bottom flooding data. Most water outlet temperatures are close to saturation, and particularly for lower water flow rates and higher inclination angles. This clearly indicates that bottom flooding, even in condensing flow, may be considered to be hydraulics-limited rather than heat-transfer-limited, as argued by Wallis *et al.* [15]. It is also seen in Fig. 2 that the prediction is in quite good agreement with the data, and that the difference between $T_{f,in} = 10$ and 100°C is almost negligible. This implies that the local condensation effect may be insignificant in altering the vapor flooding velocity, as mentioned earlier.

Figure 4 shows the top flooding data for three different water inlet temperatures in nearly vertical flow. The effective vapor flooding velocity, incorporat-

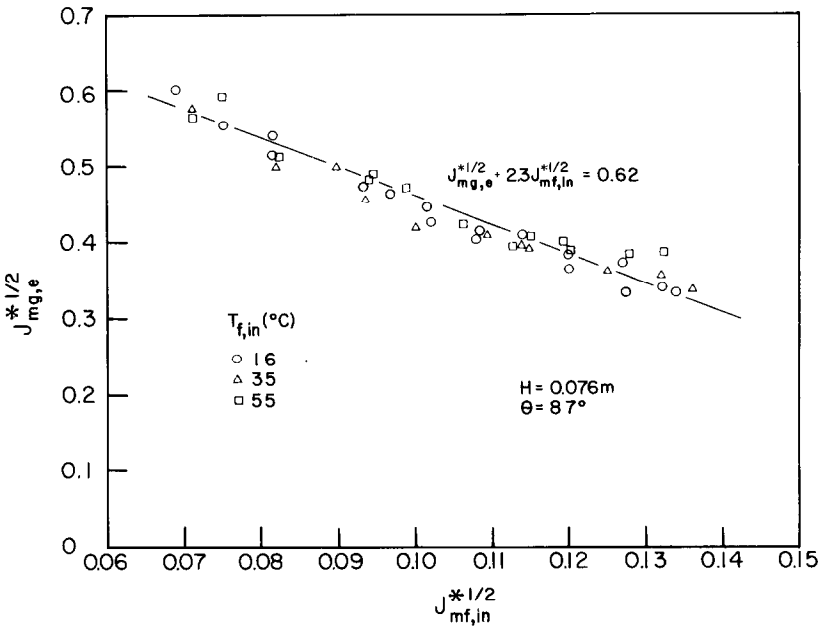

FIG. 4. Effective vapor flooding velocities for top flooding in nearly vertical flow.

ing the global effect of condensation by subtracting the condensation rate from the steam supply rate, was calculated in order to compare the data on a common basis. The dimensionless effective vapor velocity is defined by

$$J^*_{mg,e} = J^*_{mg} - f\left(\frac{\rho_f}{\rho_g}\right)^{1/2} \frac{C_{pl}(T_s - T_f)}{i_{fg}} J^*_{mf} \tag{8}$$

where the condensation efficiency, f, can be obtained from the energy balance, as follows [4]

$$f = \frac{K_{in} - K_{out}}{K_{in}(1 + K_{out})} \tag{9}$$

where K is a dimensionless subcooling number. One can see that if the exit liquid is saturated, f is identical to 1, which is true for most of the top flooding data shown in Fig. 4. It is seen that the data may be correlated by a simple linear equation in the $(J^*_{mg,e}, J^*_{mf,in})$ plane. The best fit of the data resulted in

$$J^{*1/2}_{mg,e} + 2.3J^{*1/2}_{mf,in} = 0.62. \tag{10}$$

The slope and constant in equation (10) indicate higher values than those proposed by other investigators [12–14], but this is not surprising, considering the different length scales used in the denominator of equation (7).

EFFECT OF CHANNEL DEPTH

Scaling for the onset of flooding in countercurrent stratified two-phase flow in rectangular ducts is associated with the effect of the channel depth (plate spacing), so long as essentially 2-D flow is assured. The scaling parameter, J^*_{mk}, introduced in this study has emerged from the flooding analysis based on the envelope theory. However, a similar dependence of the flooding velocity on the channel depth, as indicated in the modified Wallis parameter, may be obtained from the extended form [1] of the stability criterion proposed by Mishima and Ishii [10] for horizontal cocurrent flow.

Experimental data for two different channel depths, $H = 0.038$ and 0.076 m, are plotted in the (U_g, U_f) plane, as shown in Fig. 5. It is seen that higher vapor velocities are needed to cause the inception of flooding for larger channel depths at both inclinations. This result indicates that the instability is significantly enhanced by the proximity of the upper wall. Figure 6 shows a comparison between the envelope theory and the data for two channel depths at moderately steep angles. The envelope curves were obtained from equations (2) and (3), neglecting the condensation effect because its insignificance has already been shown in an earlier comparison. In general, good agreement between the theory and data is indicated. It is also seen in Fig. 6 that the experimental data for both channel depths tend to converge in the low J^*_{mf} region, whereas the dimensionless gas flooding velocity for $H = 0.038$ m is slightly higher in the high J^*_{mf} region. Because the interfacial friction factor in equation (2) is dependent upon the channel depth as well as the void fraction, some difference between the two flooding curves is also found. This result shows that the dependence of the channel depth on the flooding velocity may not be expressed by a single dimensionless parameter of the form of J^*_{mk}.

EFFECT OF INCLINATION ANGLE

It was observed that the onset of flooding at the nearly horizontal and moderately steep angles occurs after well-developed roll waves appear on the interface, whereas the inception of flooding in nearly vertical flow is associated with a chaotic interface and strong droplet entrainment. Distinct roll waves did not appear before

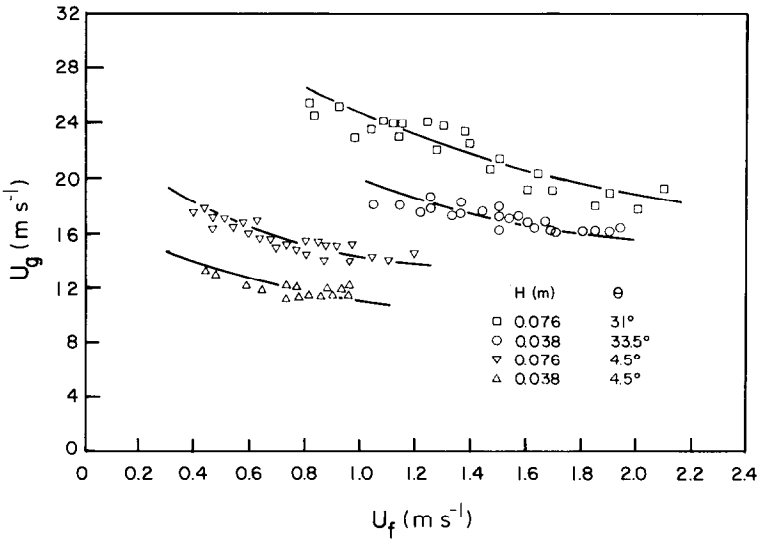

FIG. 5. Comparison of actual bottom flooding velocities for $H = 0.076$ and 0.038 m.

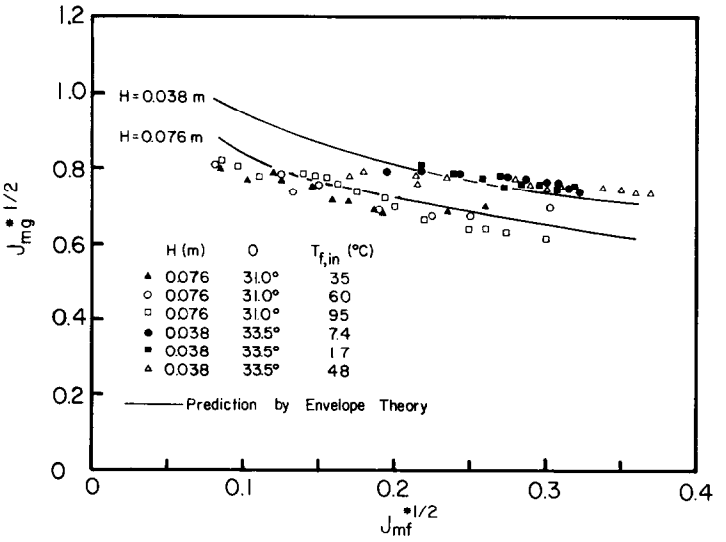

FIG. 6. Comparison of envelope theory with bottom flooding data in moderately inclined flows.

the onset of flooding at this angle. This has the interesting implication that flooding may be initiated in different modes, depending upon the inclination angle. This may also be shown by the experimental results of Hewitt [16], who performed flooding tests in inclined annular flow. As the inclination varied from horizontal to vertical, the superficial flooding velocity increased and then decreased at a fixed gas velocity, with a maximum between $\theta = 60°$ and 80° from the horizontal. This result is thought to be closely related to the effect of a stabilizing gravity force, which is predominant in controlling the motion of the interfacial wave in inclined countercurrent two-phase flow. One may speculate from these results that when $\theta < \theta^*$, where θ^* is the inclination angle where the maximum liquid flooding velocity is attained, the gravity force suppresses unstable wave growth until rough roll waves are well developed at the interface. Since flooding may be regarded as the limiting condition for countercurrent two-phase flow, which is retarded mainly by the interfacial shear stress, the flooding velocity is closely associated with the effective roughness of the interface, which is assumed to be approximately proportional to the mean film thickness. Hence, for thinner films and accordingly for larger inclination angles, the flooding velocity becomes higher when $\theta < \theta^*$.

When $\theta > \theta^*$, the interfacial wave is likely to grow relatively easily, owing to the diminished effect of the

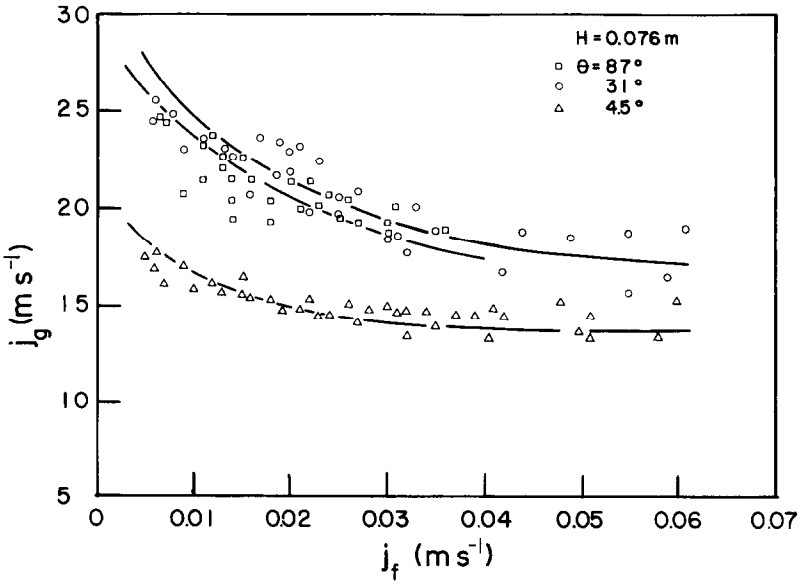

FIG. 7. Superficial bottom flooding velocities at three different angles.

gravity force, and hence the onset of flooding may be the result of unstable wave growth. However, the mechanism involved in this unstable growth is complicated because of the entrainment and redeposition of liquid droplets. The unstable wave growth is moderated by tearing off drops from the finite-amplitude waves, and redeposition onto the film and wave troughs, leading to a very chaotic flow pattern. Since an increase of inclination angle results in a decreased gravity effect, the roll waves are not stable, but instead quickly disintegrate into droplets. Thus, a pronounced appearance of roll waves before the onset of flooding is less likely, which agrees with the observations in the present experiment.

This argument appears to be partly supported by the bottom flooding data at three different angles shown in Fig. 7. Similar trends to the experimental results of Hewitt [16] are indicated. The superficial flooding velocities at $\theta = 31°$ are higher than those at $\theta = 4.5°$, but the data for nearly vertical flow ($\theta = 87°$) lie in between. However, it is noteworthy that the quantitative trend of the present data is not exactly identical to that of Hewitt [16]. For instance, the data of Hewitt at a nearly vertical angle are not necessarily lower than those at $\theta = 31°$. This is not surprising, considering the liquid entrance conditions of both experiments. In ref. [16] a considerable maldistribution of the liquid film around the circumference was noted as the inclination angle was decreased. However, in the present system uniform liquid film distribution along the bottom wall of the test section was assured using a stratified flow configuration.

A comparison between the prediction by the envelope theory and flooding data in the nearly vertical flow is shown in Fig. 8. It is seen, first of all, that the gas flooding velocities for top flooding are smaller than those for bottom flooding. This is undoubtedly because of the presence of a hydraulic jump and consequent maldistribution of the liquid film when it is purposely not introduced smoothly at the entrance for the top-flooding test. In nearly all practical cases the liquid entrance will not be smooth, so that top flooding can be expected. These effects are more significant at higher liquid flow rates, so that the difference between these data becomes considerable when the liquid flow rate is increased.

The figure shows that the prediction is, in general, higher than the flooding data. This deviation may, in part, be attributable to the significant effect of liquid entrainment at this angle. Owing to the weak stabilizing effect of the capillary force, an interfacial wave is more likely to be excited, but cannot grow to the permanent-type roll wave because the tip is easily cut off by the upwards gas flow. Physically, the envelope curve represents an ideal limiting condition for countercurrent flow, neglecting the interactions of two streams other than interfacial shear. In nearly horizontal or moderately inclined countercurrent flow (presumably $\theta > \theta^*$), the entrainment is not an important factor in causing the onset of flooding, because the considerable increase in interfacial shear stress due to the appearance of well-developed roll waves results in retardation of the liquid film. However, in nearly vertical flow ($\theta > \theta^*$) the entrainment effect appears to be important because of the weak capillary force stabilizing the interfacial wave.

Another important consideration is the use of the Bharathan friction factor correlation, equations (A4)–(A6), taken in air–water vertical annular flow, for this stratified, nearly-vertical, steam–water flow. Friction factors taken with air–water in this equipment might yield considerably better agreement.

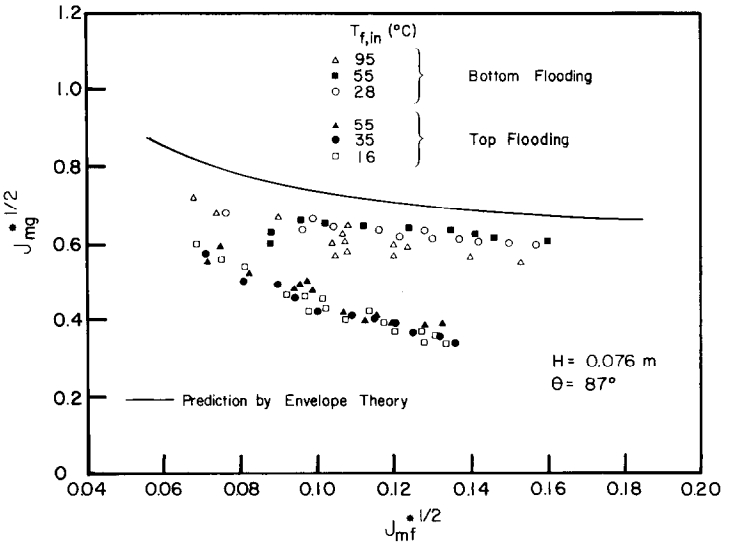

FIG. 8. Comparison of envelope theory with flooding data in nearly vertical flow.

SUMMARY AND CONCLUSIONS

Countercurrent stratified flooding in flat-plate geometries has been investigated. The envelope theory, which considers the onset of flooding to be the limiting condition for countercurrent flow, is compared with extensive data at three different inclinations. The results indicate quite good agreement between the theory and the data. Local condensation effects on the onset of flooding appears to be insignificant for the bottom flooding data, whereas the effective steam flow rate should be considered for the top flooding data in order to incorporate the global condensation effect. An increase of channel depth tends to increase the vapor flooding velocity, indicating that the instability is significantly enhanced by the proximity of the plate spacing. Flooding in the nearly horizontal and moderately-inclined flows may be regarded as the limiting condition for countercurrent flow. However, the onset of flooding in the nearly vertical flow was expedited by significant droplet entrainment, and thus took place before well-developed roll waves appeared at the interface. Finally, the liquid entrance condition seems to play an important role in determining the flooding velocity, as seen from a comparison of the bottom and top flooding data.

Acknowledgement—This work was supported by the U.S. Nuclear Regulatory Commission.

REFERENCES

1. S. G. Bankoff and S. C. Lee, A critical review of the flooding literature, in *Multiphase Science and Technology* (edited by G. F. Hewitt, J. M. Delhaye and N. Zuber). Hemisphere, Washington, DC (in press).
2. G. B. Wallis, Flooding velocities for air and water in vertical tubes, UKAEA Report, AEEW-R123 (1961).
3. S. S. Kutateladze, Elements of the hydrodynamics of gas–liquid systems, *Fluid Mech.–Sov. Res.* **1**, 29–50 (1972).
4. S. C. Lee, Stability of steam–water countercurrent stratified flow, Ph.D. thesis, Northwestern University, Evanston, Illinois (1983).
5. S. C. Lee and S. G. Bankoff, Stability of steam–water countercurrent flow in an inclined channel: I. Flooding, *Trans. Am. Soc. Mech. Engrs*, Series C, *J. Heat Transfer* **105**, 713–18 (1983).
6. H. Imura, H. Kusuda and S. Funatsu, Flooding velocity in a countercurrent annular two-phase flow, *Chem. Engng Sci.* **32**, 79–87 (1977).
7. A. G. Cetinbudaklar and G. J. Jameson, The mechanism of flooding in vertical countercurrent two-phase flow, *Chem. Engng Sci.* **24**, 1669–1680 (1969).
8. N. S. Hall-Taylor and R. M. Nedderman, The coalescence of disturbance waves in annular two-phase flow, *Chem. Engng Sci.* **23**, 551–564 (1968).
9. A. S. Telles and A. E. Dukler, Statistical characteristics of thin vertical wavy liquid films, *Ind. Engng Chem. Fundam.* **9**, 412–421 (1970).
10. K. Mishima and M. Ishii, Theoretical prediction of onset of horizontal slug flow, *J. Fluid Engng* **102**, 441–445 (1980).
11. D. Bharathan, G. B. Wallis and H. J. Richter, Air–water countercurrent annular flow, EPRI-NP-1165 (1979).
12. S. G. Bankoff, R. S. Tankin, M. C. Yuen and C. L. Hsieh, Countercurrent flow of air–water and steam–water through a horizontal perforated plate, *Int. J. Heat Mass Transfer* **24**, 1381–1395 (1981).
13. P. H. Rothe and C. J. Crowley, Scaling of pressure and subcooling for countercurrent flow, NUREG/CR-0464 (1978).
14. C. L. Tien, A simplified analytical model for countercurrent flow limiting phenomena with condensation, *Lett. Heat Mass Transfer* **4**, 231–238 (1977).
15. G. B. Wallis, D. C. deSieyes, R. J. Rosselli and J. Lacombe, Countercurrent annular flow regimes for steam and subcooled water in a vertical tube, EPRI-NP-1336 (1980).
16. G. F. Hewitt, Influence of end conditions, tube inclination and physical properties on flooding in gas–liquid flow, Harwell Report, HTFS-RS 222 (1977).
17. S. G. Bankoff and H. J. Kim, Direct-contact condensation of steam on cold water in stratified countercurrent flow, Topical Report to U.S. NRC (in press).

APPENDIX

Equations and empirical correlations used in the present analysis are listed in this section.

(1) Liquid sidewall friction factor [4]

$$1.0-3.0\sqrt{\left(\frac{f_{wf}}{2}\right)}=2.5\sqrt{\left(\frac{f_{wf}}{2}\right)}\ln\left(Re_f\sqrt{\left(\frac{f_{wf}}{2}\right)}\right)-\frac{64}{Re_f}. \quad \text{(A1)}$$

(2) Steam sidewall friction factor (Blasius equation)

$$f_{wg}=0.0559Re_g^{-1/4}. \quad \text{(A2)}$$

(3) Adiabatic interfacial friction factor [4, 11]:

for $H = 0.076$ m and $\theta = 4.5°$

$$f_{ia}=0.012+6.09\times10^{-8}(1-\alpha)^{2.54}N_{mf}^{0.85}\times[N_{mg}J_{mg}^{*}-1.84(N_{mf}J_{mf}^{*})^{-0.184}]; \quad \text{(A3)}$$

for moderately steep and nearly vertical angles

$$f_{ia}=0.005+A(H^{*}/2)^{B}(1-\sqrt{\alpha})^{B} \quad \text{(A4)}$$

$$\log A=-0.56+9.07/H^{*} \quad \text{(A5)}$$

$$B=1.63+4.74/H^{*}. \quad \text{(A6)}$$

(4) Local heat transfer coefficient [17]

$$Nu^{*}=Nu(x/\delta) \quad \text{(A7)}$$

$$Nu=A\,Re_g^{e_1}\,Re_f^{e_2}\,Pr^{e_3} \quad \text{(A8)}$$

where for $H = 0.076$ m and $\theta = 4.5°$

$$A=6.3\times10^{-6};\ e_1=0.9;\ e_2=0.74;\ e_3=0.81$$

for $H = 0.076$ m and $\theta = 31°$

$$A=1.35\times10^{-4};\ e_1=0.35;\ e_2=1.0;\ e_3=0.56$$

for $H = 0.038$ m and $\theta = 33.5°$

$$A=3.43\times10^{-10};\ e_1=2.1;\ e_2=0.56;\ e_3=1.16.$$

(5) Mean film thickness [4]

$$\delta^{*}=0.304Re_f^{7/12} \quad \text{(A9)}$$

where the dimensionless film thickness is defined by

$$\delta^{*}=\delta[\rho_f(\rho_f-\rho_g)g\sin\theta/\mu_f^{2}]^{1/3}. \quad \text{(A10)}$$

EFFETS PARAMETRIQUES SUR L'APPARITION DE L'ENGORGEMENT DANS LES GEOMETRIES DE PLAQUES PLANES

Résumé—On étudie l'engorgement de l'écoulement vapeur d'eau–eau stratifié à contre-courant dans des géométries de plaques planes. On discute à la fois les effets locaux et globaux de la condensation sur l'apparition de l'engorgement, à partir des résultats d'essais. L'influence de la profondeur du canal et de l'angle d'inclinaison sur la vitesse d'engorgement est analysée. Un modèle d'enveloppe qui considère l'engorgement comme la condition limitant l'écoulement à contre-courant, est présenté et comparé avec des données obtenues à différents inclinaisons. Un assez bon accord est obtenu pour les inclinaisons modérées ou nulles, mais l'engorgement dans les écoulements presque verticaux sont compliqués par l'entrainement de gouttelettes et il apparait plus tôt que ne le prévoit la théorie.

PARAMETRISCHE EINFLÜSSE AUF DAS EINSETZEN DES FLUTENS VON EBENEN FLÄCHEN

Zusammenfassung—Das Fluten von ebenen Flächen bei gegenläufigen geschichteten Dampf-Wasserströmen wird untersucht. Sowohl örtliche als auch übergreifende Auswirkungen der Kondensation auf das Einsetzen des Flutens werden, gestützt auf Versuche mit Fluten von oben und von unten diskutiert. Der Einfluß von Kanaltiefe und heigungswinkel auf die Flutgeschwindigkeit wird untersucht. Es wird ein Grenzwertmodell vorgestellt, das das Fluten als Grenzfall für gegenläufige Strömungen betrachtet. Das Modell wird mit umfangreichen Daten bei verschiedenen Neigungswinkeln verglichen. Für fast horizontale und mäßige Neigungen wird recht gute Übereinstimmung beobachtet, bei nahezu senkrechter Anordnung wird das Einsetzen des Flutens durch beträchtlichen Tropfeneintrag beschleunigt und tritt dadurch eher als nach der Theorie auf.

ВЛИЯНИЕ ЗНАЧЕНИЙ НЕКОТОРЫХ ПАРАМЕТРОВ НА НАЧАЛО ЗАТОПЛЕНИЯ В ГЕОМЕТРИЯХ С ПЛОСКИМИ ПЛАСТИНАМИ

Аннотация—Исследуется явление затопления при стратифицированном пароводяном течении в противотоке в геометриях с плоскими пластинами. На основе опытов по верхнему и нижнему затоплению обсуждается влияние как локальной, так и суммарной конденсации на начало затопления. Также исследуется влияние на скорость затопления глубины канала и угла его наклона. Представлена модель, в которой затопление рассматривается как предельное условие при течении в противотоке, и проведено сравнение с многочисленными данными, полученными при различных углах наклона. Получено довольно хорошее совпадение данных при почти горизонтальном положении канала и при не очень большом его наклоне. Начало затопления в почти вертикальном канале сопровождается значительным уносом капель, в результате чего оно наступает раньше, чем это предсказывает теория.